

Performance of novel dynamic installed anchors during installation and monotonic pullout

Youngho Kim* and Lachlan Thomas Rosher^a

Centre for Offshore Foundation Systems (COFS), The University of Western Australia, 35 Stirling highway, Crawley, WA 6009, Australia

(Received November 13, 2018, Revised May 12, 2019, Accepted May 13, 2019)

Abstract. This paper examines the results from three-dimensional dynamic finite element analysis undertaken to develop a new dynamically installed anchor (DIA). Several candidate shapes of new DIAs were selected after an investigation into previous researches of existing DIA designs. The performances of selected DIAs during the installation and loading in non-homogeneous clay were investigated through large deformation finite element (LDFE) analyses. Findings were compared to the current anchors in operation (i.e., Torpedo and Omni-Max DIA) to assess the viability of the new designs in the field. Overall, the anchor embedment depths of the novel DIAs lied under the results of OMNI-Max DIA. And also, the tracked anchor trajectory confirmed that, the novel DIAs dove deeper with stiffer travelling angle, compared to the OMNI-Max DIA. These elements are more critical and beneficial especially in a field where the achieved embedment depths are generally low.

Keywords: anchors; clays; numerical modelling; offshore engineering

1. Introduction

The increase in global demand for both oil and gas has resulted in a significant depletion in shallow water resources. Accordingly, there has been a recent influx of research and resources exploring cost-effective solutions to operating in deep and ultra-deep water. For water depths greater than 500 m, it becomes difficult to create structures with natural frequencies that do not cause resonance disaster from oscillating due to the unbalanced wave frequency (Aubeny *et al.* 2001). As a result, anchoring has become an increasingly important part of the development scenarios in deep sea. Conventional anchoring solutions for these deep sea developments include (a) suction caissons (Muduli *et al.* 2015, Lee *et al.* 2015); (b) plate anchors (Bhattacharya and Roy 2016, Emirler *et al.* 2016, Bhattacharya 2017, Bhattacharya and Sahoo 2017). Dynamically installed anchors (DIAs) are the most recent generation of anchoring systems for mooring floating facilities in deep waters. DIAs have been identified as one of the most cost-effective and promising concepts for future oil and gas development in the emerging frontiers. They are also being increasingly considered in shallow waters for temporary mooring of floating facilities and for mooring floating wind turbines and wave energy converters (Choi *et al.* 2015, Kim *et al.* 2015).

As shown in Fig. 1a the DIA is released from a specified height above the seabed. This allows the anchor to gain velocity as it falls freely through the water column before impacting the seafloor and embedding into the sediments, without external energy source or mechanical operation

(O'Loughlin *et al.* 2009, Lieng *et al.* 2010). Moreover, the deeper embedment depths of DIAs guarantee higher pullout capacity due to the increase in seabed shear strength (Richardson *et al.* 2009, O'Loughlin *et al.* 2013, Hossain *et al.* 2014, 2015, Kim and Hossain 2016). So, it would be especially beneficial if the new DIA can penetrate deeper than existing design shapes. The main parameters that govern the penetration of a DIA in the given seabed condition include (a) the anchor weight, (b) the drop height and hence impact velocity, (c) the anchor geometry (Richardson *et al.* 2009, O'Loughlin *et al.* 2013, Kim *et al.* 2015a).

The recently developed DIA, such as the OMNI-Max (Shelton *et al.* 2011), was designed by shifting the padeye towards its tip at approximately 2/3 of the anchor length for better keying and potential diving in soil upon pullout loading. Several studies already have demonstrated that this lowered padeye position may allow the anchor to embed further (through diving) during pullout loading (Tian *et al.* 2014, Liu *et al.* 2016, Zhao *et al.* 2016, Kim and Hossain 2017, Chang *et al.* 2018, Kim *et al.* 2018, see Fig. 1(b)). The diving behaviour would distinctly increase anchor's pullout capacity and mitigate the risk of catastrophic failure (Zimmeman *et al.*, 2009). The key aspects that relate to the DIA's ability to dive are (a) location of centroid mass; (b) padeye offset ratio; and (c) pullout angle (Kim and Hossain 2017).

The motivation of this study has emanated directly from the need identified by the offshore industry in an attempt to extend the application of DIAs in untested environments. Therefore, the main objective is to develop the new DIA shapes to be measured with which performs the most effectively, with installation depth and diving performance, as well as cost efficiency in design. This development process builds on previous researches for the existing DIAs.

*Corresponding author, Ph.D.
E-mail: youngho.kim@uwa.edu.au

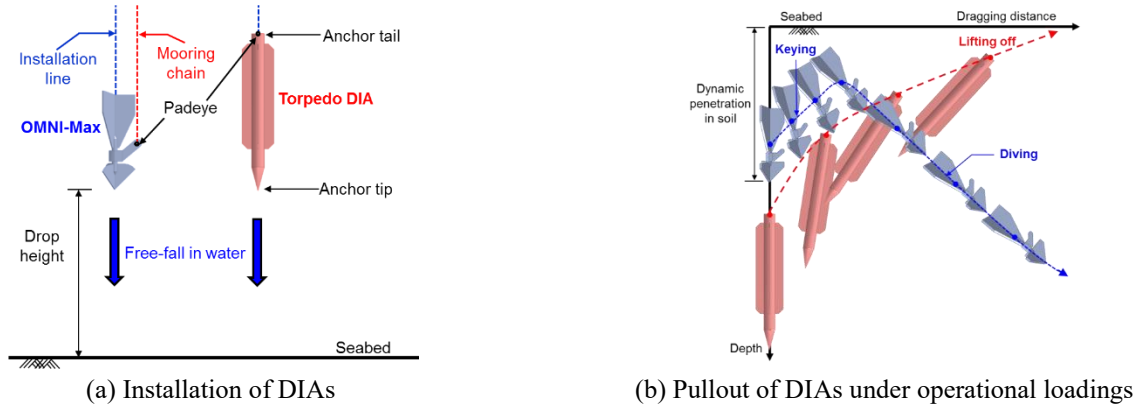


Fig. 1 Behaviours of DIAs

Table 1 Preliminary concept for a new DIA shape

Anchor	A1	A2	A3	A4	A5
Drawing					
Inspiration	Arrowhead	Arrowhead	Nail / Bolt	Combined A1 and A2	Combined A1 ~ A3
Advantage	Small projected area (A_p)	Small A_p	Small A_p	Low h_c and small A_p	Low h_c
Limitation	High centroid mass location (h_c)	High h_c	High h_c and fabrication cost	Structural integrity	Large A_p
Expected penetration depth	Deep	Deep	Deep	Deep	Shallow
Expected diving potential	No diving	No diving	No diving	Diving	Diving

Several candidate shapes of new DIAs were selected from the previous researches of existing DIA designs. The performances of selected DIAs during the installation and loading in non-homogeneous clay were investigated through three-dimensional (3D) dynamic LDFE analyses. To assess the viability of the new DIA shapes, an extensive comparative investigation against existing DIAs was undertaken, varying the relevant range of various parameters related to the impact velocity and pullout inclination angle. A simple measure of cost efficiency between various anchor designs was then considered to be the ratio of the holding capacity versus the weight of materials of the anchor.

2. Numerical analysis

2.1 DIA geometry and parameters

Taking into consideration the advantages from the existing DIAs, a series of anchor models were formed with the desire for a novel anchor shape which performs well respecting performance in both installation and pullout. Total five models were created and refined using ABAQUS (Version 6.12, Dassault Systèmes 2012). These preliminary

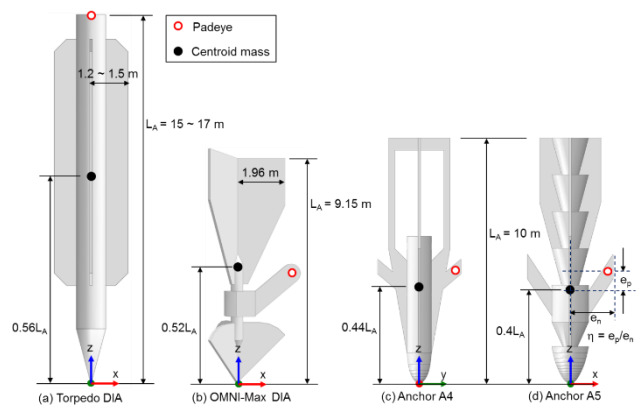


Fig. 2 Schematic geometries of existing DIAs and novel anchors: (a) Torpedo DIA, (b) OMNI-Max DIA, (c) Anchor A4 and (d) Anchor A5

models, which took inspiration from existing anchors in the field and also other real world objects (e.g., arrowhead, nail etc.) can be seen in Table 1. The key aim of the novel anchor shape was looked for maximising the penetration depth and diving potential of DIAs. The software aided in the location of points such as the centre of mass and other properties such as the projected surface area. Using this information, the anchors A4 and A5 were selected due to

Table 2 Preliminary concept for a new DIA shape

Description	Symbol (unit)	OMNI-Max	Finless torpedo	Anchor A4	Anchor A5
Total anchor length	L_A (m)	9.15	10	10	10
Fin thickness	t_f (m)	0.1	-	0.1	0.1
Anchor frontal projected area	A_p (m ²)	1.91	0.79	1.23	2.18
DIA volume	V_A (m ³)	5.02	6.8	6.76	7.83
DIA submerged weight	W_s (kN)	341	341	341	341
Location of centroid mass	h_c (m)	4.76	5.5	4.4	4.0
Padeye offset	e_p (m)	0.68	-	0.14	0.45
Padeye eccentricity	e_n (m)	1.96	-	1.5	1.55
Padeye offset ratio	η^*	0.35	-	0.09	0.3

* $\eta = e_p/e_n$ (see Fig. 2)

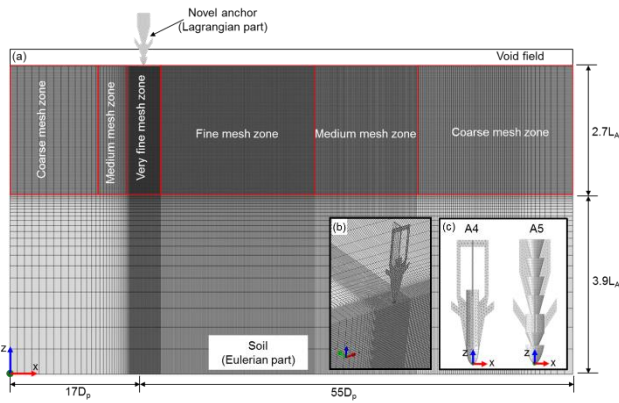


Fig. 3 Typical mesh used in 3D LDFE analysis: (a) Side view, (b) 3D view and (c) Anchor modelling

their low centre of mass, small projected surface area, slender profile and relatively simple construction. To reduce the comparison cases, the submerged weight (W_s), total length (L_A) and fin thickness (t_f) of new DIA were kept as constant. These are illustrated in Fig. 2 with comparisons of existing DIAs, and dimensions are given in Table 2.

2.2 Numerical simulation procedure

3D LDFE analyses were carried out using the Coupled Eulerian-Lagrangian (CEL) approach in the commercial finite element package ABAQUS/Explicit (Dassault Systèmes 2012). Extensive background information about installation and pullout modelling of DIAs can be found in Kim *et al.* (2015a) and Kim and Hossain (2015, 2017), which are not repeated here.

Considering the symmetry of the problem, only a half anchor and soil domain were modelled. The lateral extension of the soil domain were $55D_p$ from the centre of the anchor (D_p is the anchor frontal projected area (A_p) equivalent diameter) on the pullout loading direction and $17D_p$ on the opposite respectively. A typical mesh is shown in Fig. 3. The Eulerian mesh comprised 8-noded linear brick elements (termed EC3D8R in ABAQUS) with

reduced integration. As obtained from preliminary convergence studies (e.g., Kim and Hossain 2017 and Kim *et al.* 2018), the typical minimum soil element size along the trajectory of the anchor was selected as $0.18t_f$ (where t_f is the anchor fin thickness) for vertical installation (very fine mesh zone) and $0.5t_f$ for inclined pullout (fine mesh zone). The anchor was simplified as a rigid body.

The simulation was fully integrated taking into account the disturbed soil conditions during the installation of the anchor for the pullout stage (Kim and Hossain 2016). In this study, an inclined pullout loading, rather than an inclined displacement, was applied to the anchor padeye (θ_a) to obtain apparent anchor trajectory. The pullout process of anchors in clay is completed under undrained conditions. The soil was thus modelled as an elasto-plastic material obeying a Tresca yield criterion, but extended to capture strain-rate and strain-softening effects, following the models of Einav-Randolph (Einav & Randolph 2005).

$$s_u = \left[1 + \lambda \log \left(\frac{\text{Max}(|\dot{\gamma}|, \dot{\gamma}_{ref})}{\dot{\gamma}_{ref}} \right) \right] \left[\delta_{rem} + (1 - \delta_{rem}) e^{-3z/\zeta_{95}} \right] s_{u,ref} \quad (1)$$

The definitions are given under notation list, with the details reported by Hossain and Randolph (2009), Zheng *et al.* (2015) and Kim and Hossain (2017). The elastic behaviour was defined by a Poisson's ratio of 0.49 and Young's modulus of $500s_u$ throughout the soil profile. The soil-anchor interface was modelled as frictional contact with a limiting shear stress (τ_{max}) along the anchor-soil interface. Typical computation times on a high performance workstation with 12 CPU cores were about a week for an anchor dynamic installation followed by monotonic pullout of ~ 2 anchor lengths.

3. Results and discussion

To examine the effect of various factors on the performances of novel DIAs, an extensive parametric study was carried out varying (a) impact velocity; and (b) loading angle. The soil undrained shear strength and soil sensitivity adopted a reported values ($s_{u,ref} = 2.4 + 1.1z$ kPa; $S_t = 3$) at the Gulf of Mexico (Zimmerman *et al.*, 2009), where OMNI-Max DIAs were installed. Parameters in terms of rate dependency and strain-softening were taken as $\lambda = 0.1$; $\dot{\gamma}_{ref} = 1.5\% \text{ h}^{-1}$ $\zeta_{95} = 20$, as they provided good match in the previous validation exercise (Kim and Hossain 2017; Kim *et al.* 2018). The results from this parametric study, as assembled in Table 3, are discussed below.

3.1 Penetration efficiency during installation

As mentioned earlier, the penetration of a DIA is a function of impact velocity, anchor weight, anchor geometry (i.e., projected and anchor-soil contact surface area) and undrained shear strength of the surrounding soil (O'Loughlin *et al.* 2013, Hossain *et al.* 2015, Kim *et al.* 2015b).

Fig. 4 shows the anchor penetration profiles for selected novel DIAs (anchors A4 and A5; Table 1), as a function of time and velocity of anchor, in soft clay with $s_{u,ref} = 2.4 +$

Table 3 Summary of 3D LDFE analyses performed

Group	Anchor	$S_{u,ref}$ (kPa)	v_i (m/s)	$d_{e,t}$ (m)	θ_a (deg.)	ϕ (deg.)	Note		
I	Anchor A4	2.4 + 1.1z	19	22.72	-	-	- Comparison with penetration depth		
	Anchor A5			18.1					
	Finless torpedo			34.95					
	OMNI-Max			16.87					
II	Anchor A4	2.4 + 1.1z	7	16.89	30	-23.3	- Comparison with diving potential during loading		
	Anchor A5		16.5	16.91		-20.1			
	OMNI-Max		19	16.87		-15.8			
III	Anchor A4	2.4 + 1.1z	7	16.89	15	-45.3	- Effect of pullout angle		
	Anchor A5				16.5	16.91		45	Lifted off
	Anchor A5				16.5	16.91		45	Lifted off
	OMNI-Max				19	16.87		45	Lifted off

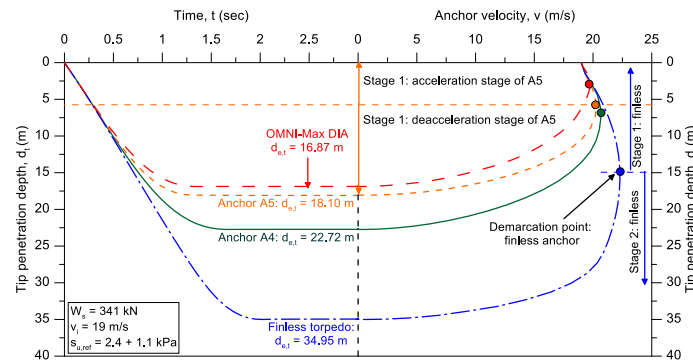


Fig. 4 Penetration profiles for various DIAs

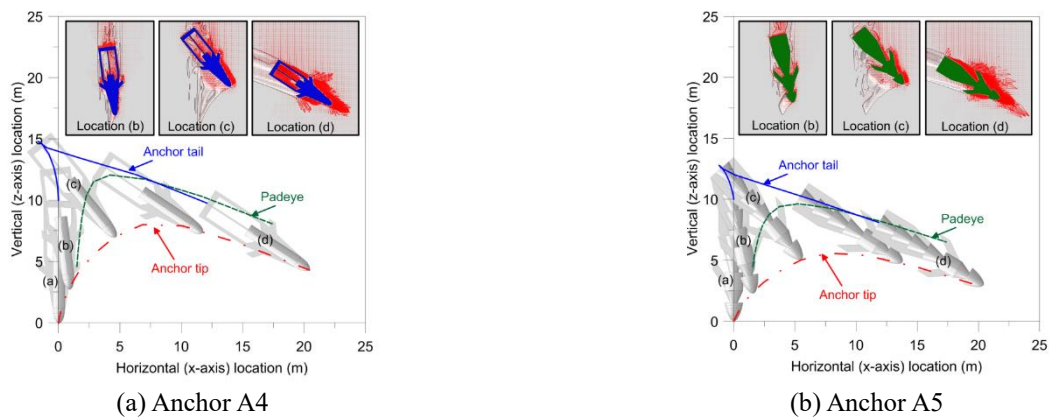


Fig. 5 Typical novel anchor diving trajectories and corresponding failure mechanisms

1.1z kPa. To assess the penetration capability of new anchor shapes, the finless torpedo and OMNI-Max DIAs are plotted together (Group I in Table 3). The impact velocity (v_i) was a constant of $v_i = 19$ m/s for all cases. Generally, the DIA penetration profile can be divided into two stages (see Fig. 4). Stage 1 corresponds to shallow penetration where the DIA accelerates although it advances into the soil. The soil resistance is less than the submerged weight of the anchor. In stage 2, at greater penetration, the frictional

and end bearing resistance, along with the inertial drag, outweigh the submerged weight and the DIA decelerates (Kim *et al.* 2015a). These different penetration stages were also indicated in Fig. 4.

Generally, the DIA penetration profile can be divided into two stages (see Fig. 4). Stage 1 corresponds to shallow penetration where the DIA accelerates although it advances into the soil. The soil resistance is less than the submerged weight of the anchor. In stage 2, at greater penetration, the

frictional and end bearing resistance, along with the inertial drag, outweigh the submerged weight and the DIA decelerates (Kim *et al.* 2015a). These different penetration stages were also indicated in Fig. 4.

Overall, compared to the OMNI-Max DIA, the both novel DIAs are able to penetrate deeper at the same impact velocity (v_i) and soil strength ($S_{u,ref}$). For example, penetration ratios for both new DIAs ($d_{e,t} = 18.1 \text{ m} \sim 22.72 \text{ m}$) are greater than the previous results for OMNI-Max DIA ($d_{e,t} = 16.87 \text{ m}$). This means that from a purely installation perspective, they outperform the existing OMNI-Max DIA under the similar environmental condition. This is attributed to the streamline body and small projected area (A_p) of novel DIAs. Especially, the latter was demonstrated to have the greatest influence on the penetration performance (Richardson *et al.* 2009, Kim *et al.* 2015a). The large projected area mobilises the greater vertical soil resistance the soil, which results in the shorter acceleration stage (stage 1) and hence the shallow penetration depth (see Fig. 4). That is why the finless torpedo DIA with the smallest projected area recorded the deepest embedment depth ($d_{e,t} = 34.95 \text{ m}$) in this comparison plot (see Fig. 4). Note, the finless torpedo DIA is well known for its significant low pullout capacity, compared to other types of DIAs (Kim *et al.* 2016). Therefore, only OMNI-Max DIA was used as a reference case for subsequent pullout analyses.

3.2 Pulling out performance

3.2.1 Diving potential and corresponding failure mechanisms

In order to allow for a direct comparison between the novel DIAs and the OMNI-Max DIA, the embedment depth ($d_{e,t}$) should be identical. Based on the previous results for the OMNI-Max data (Kim and Hossain 2015), the embedment depth of the novel DIAs was adjusted to be close ($d_{e,t} \approx 16.9 \text{ m}$) by impact velocity (Group II in Table 3). With a similar embedment depths, the anchors were then pulled out at an angle of $\theta_a = 30^\circ$.

Fig. 5 depicts the typical diving trajectories and corresponding failure mechanisms. It shows the pullout track of the new DIAs can be divided into two main stages: (i) keying; (ii) diving. At the beginning of the keying process (between location (a) and location (c) in Fig. 5), the soil adjacent to the DIA head fins (tip) moves significantly and faster, while the soil around to the DIA tail fins moves marginally (see inset figure). This indicates that the DIA rotates or keying occurs at this stage. At the end of the keying process (location (c) in Fig. 5), more mobilisation of soil movement can be seen around to the DIA tail fins, indicating translation of the DIA with minor rotation. In the diving stage (location (d) in Fig. 5), the DIA moves into deeper soil with a constant angle (defined as ϕ ; see Fig. 2), and a significant soil movement occurs around the DIA.

Fig. 6 shows the centroid traveling direction and corresponding stabilised travelling angle (ϕ) of the novel DIAs (anchors A4 and A5) and OMNI-Max DIA. Overall, all the DIAs show a similar pullout trajectory path, including keying and diving. However, in terms of diving efficiency, the anchor A5 provides the better performance, compared to the other DIAs. As shown in figure, the anchor

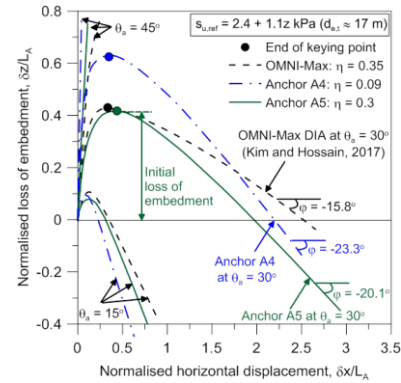


Fig. 6 Diving efficiency during loadings

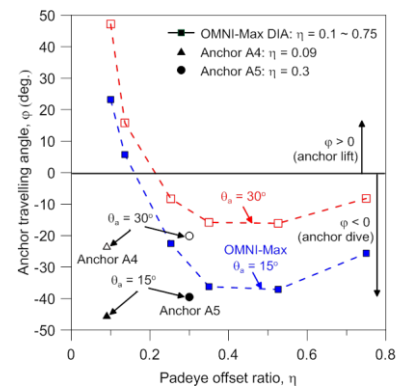


Fig. 7 Design chart for anchor travelling angle as a function of padeye offset ratio and load inclination at padeye

A5 dives earlier than the anchor A4 and deeper than the OMNI-Max DIA. These mean that the shape of anchor A5 results in an earlier transition of diving directions (i.e., initial loss of embedment depth) with stiff travelling angle i.e., ϕ . As mentioned earlier, the diving potential of anchor can be determined by the combination effect between the location of centroid mass and padeye offset ratio, if the pullout angle is constant (Tian *et al.* 2015, Liu *et al.* 2016, Kim and Hossain 2017). The current results of trajectory paths are also consistent to these principals from the previous researches. Anchor A4 has a very low padeye offset ratio ($\eta = 0.09$), compared to other DIAs ($\eta = 0.3 \sim 0.35$). For this reason, anchor A4 shows the largest initial loss of embedment depth, although it has the low centroid mass location.

3.2.2 Effect of pullout angle

Additionally, to show the effect of pullout angle (θ_a), anchor trajectories for $\theta_a = 15^\circ$ and 45° (Groups III, Table 3) are also plotted in Fig. 6. Overall, for all the DIAs, the stabilised centroid travelling angle (ϕ is getting stiffer with reducing pullout angle (θ_a)). Furthermore, the results suggest that the all the DIAs always lift up for load pulling angles of more than 45° . As shown in Fig. 7, Liu *et al.* (2016) and Kim and Hossain (2017) suggested a design chart for the OMNI-Max DIA, considering the relationship between the stabilised travelling angle (ϕ) and the padeye offset ratio (η). The figure is divided into two zones, $\phi < 0$ indicates the DIA will dive into deeper soil, and $\phi > 0$ indicates the DIA

will lift up. All the results from this study are plotted in the design chart. Compared to a similar padeye offset ratio (η), the diving efficiency of both novel DIAs (anchor A4 and A5) significantly higher than the OMNI-Max DIA. For example, for $\eta=0.09$ (e.g., anchor A4), novel DIA dive deeper, whereas the OMNI-Max lifts up. For $\eta=0.3$ (e.g., anchor A5), novel DIA also shows about 20% stiffer diving angle than that of OMNI-Max DIA.

4. Conclusions

This paper has reported the results from three-dimensional dynamic finite element analysis undertaken on novel DIAs aiming at introducing the new DIA and assessing its performance, against other DIAs, during dynamic installation and monotonic pullout in non-homogeneous clay. Clearly, (i) during dynamic installation, the achieved embedment depths of the novel DIAs lied under the result of the OMNI-Max DIA, and (ii) during monotonic pullout, the novel DIAs dove deeper with stiffer travelling angle. These are more critical and beneficial for the field where the achieved embedment depths are generally low.

In this study, the analyses were performed considering a rigid anchor, which has no deformations during the installation and pullout. Further analyses of structure integrity for a new anchor shape are on-going and will be published in the future.

Acknowledgments

The work forms part of the activities of the Centre for Offshore Foundation Systems (COFS), currently supported as a node of the Australian Research Council Centre of Excellence for Geotechnical Science and Engineering and as a Centre of Excellence by the Lloyd's Register Foundation.

References

- Aubeny, C. Murff, J. and Roesset, J. (2001), "Geotechnical issues in deep and ultra deep waters", *Int. J. Geomech.*, **1**(2), 225-247. <https://doi.org/10.1080/15323640108500154>.
- Bhattacharya, P. (2017), "Pullout capacity of shallow inclined anchor in anisotropic and nonhomogeneous undrained clay", *Geomech. Eng.*, **13**(5), 825-844. <https://doi.org/10.12989/gae.2017.13.5.825>.
- Bhattacharya, P. and Roy, A. (2016), "Improvement in uplift capacity of horizontal circular anchor plate in undrained clay by granular column", *Geomech. Eng.*, **10**(5), 617-633. <https://doi.org/10.12989/gae.2016.10.5.617>.
- Bhattacharya, P. and Sahoo, S. (2017), "Uplift capacity of horizontal anchor plate embedded near to the cohesionless slope by limit analysis", *Geomech. Eng.*, **13**(4), 701-714. <https://doi.org/10.12989/gae.2017.13.4.701>.
- Chang, K. Hossain, M.S., Kim, Y.H. and Randolph, M.F. (2018), "Novel dynamically installed fish anchor-diving upon pullout in calcareous silt", *Proceedings of the Offshore Technology Conference*, Houston, Texas, U.S.A., April-May.
- Choi, E.Y., Cho, J.R., Cho, Y.U., Jeong, W.B., Lee, S.B., Hong, S.P. and Chun, H.H. (2015), "Numerical and experimental study on dynamic response of moored spar-type scale platform for floating offshore wind turbine", *Struct. Eng. Mech.*, **54**(5), 909-922. <https://doi.org/10.12989/sem.2015.54.5.909>.
- Dassault Systèmes (2012), *ABAQUS, Version 6.12 EF Documentation*, Hibbit, Karlsson and Sorensen, Inc., Rhode Island, U.S.A.
- Einav, I. and Randolph, M.F. (2005), "Combining upper bound and strain path methods for evaluating penetration resistance", *Int. J. Numer. Meth. Eng.*, **63**(14), 1991-2016. <https://doi.org/10.1002/nme.1350>.
- Emirler, B., Tolun, M. and Laman, M. (2016), "Experimental investigation of the uplift capacity of group anchor plates embedded in sand", *Geomech. Eng.*, **11**(5), 691-711. <https://doi.org/10.12989/gae.2016.11.5.691>.
- Hossain, M.S. and Randolph, M.F. (2009), "Effect of strain rate and strain softening on the penetration resistance of spudcan foundations on clay", *Int. J. Geomech.*, **9**(3), 122-132. [https://doi.org/10.1061/\(ASCE\)1532-3641\(2009\)9:3\(122\)](https://doi.org/10.1061/(ASCE)1532-3641(2009)9:3(122)).
- Hossain, M.S., Kim, Y.H. and Gaudin, C. (2014), "Experimental investigation of installation and pull-out of dynamically penetrating anchors in clay and silt", *J. Geotech. Geoenviron. Eng.*, **140**(7), 04014026. [https://doi.org/10.1061/\(ASCE\)GT.1943-5606.0001100](https://doi.org/10.1061/(ASCE)GT.1943-5606.0001100).
- Hossain, M.S., O'Loughlin, C. and Kim, Y.H. (2015), "Dynamic installation and monotonic pullout of a torpedo anchor in calcareous silt", *Géotechnique*, **65**(2), 77-90. <https://doi.org/10.1680/geot.13.P153>.
- Kim, B.W., Hong, S.Y., Sung, H.G. and Hong, S.W. (2015), "Comparison of simplified model and FEM model in coupled analysis of floating wind turbine", *Ocean Syst. Eng.*, **5**(3), 221-243. <https://doi.org/10.12989/ose.2015.5.3.221>.
- Kim, Y.H. and Hossain, M.S. (2015), "Dynamic installation of OMNI-Max anchors in clay: numerical analysis", *Géotechnique*, **65**(12), 1029-1037. <https://doi.org/10.1680/jgeot.15.T.008>.
- Kim, Y.H. and Hossain, M.S. (2016), "Numerical study on pull-out capacity of torpedo anchors in clay", *Géotech. Lett.*, **6**(4), 1-8. <https://doi.org/10.1680/jgele.16.00106>.
- Kim, Y.H. and Hossain, M.S. (2017), "Dynamic installation, keying and diving of OMNI-Max anchors in clay", *Géotechnique*, **67**(1), 78-85. <http://dx.doi.org/10.1680/jgeot.16.T.008>.
- Kim, Y.H., Hossain, M.S. and Chang, K. (2018), "Numerical investigation of novel dynamic installed anchors in clay and calcareous silt", *Ocean Eng.*, **163**, 29-39. <https://doi.org/10.1016/j.oceaneng.2018.05.051>.
- Kim, Y.H., Hossain, M.S. and Wang, D. (2015b), "Effect of strain rate and strain softening on embedment depth of a torpedo anchor in clay", *Ocean Eng.*, **108**, 704-715. <https://doi.org/10.1016/j.oceaneng.2015.07.067>.
- Kim, Y.H., Hossain, M.S., Wang, D. and Randolph, M.F. (2015a), "Numerical investigation of dynamic installation of torpedo anchors in clay", *Ocean Eng.*, **108**, 820-832. <https://doi.org/10.1016/j.oceaneng.2015.08.033>.
- Lee, S.Y., Huynh, T.C. and Kim, J.T. (2015), "Structural identification of gravity-type caisson structure via vibration feature analysis", *Smart Struct. Syst.*, **15**(2), 259-281. <https://doi.org/10.12989/sss.2015.15.2.259>.
- Lieng, J.T., Tjelta, T.I. and Skaugset, K. (2010), "Installation of two prototype deep penetrating anchors at the Gjoa Field in the North Sea", *Proceedings of the Offshore Technology Conference*, Houston, Texas, U.S.A., May.
- Liu, J., Lu, L. and Hu, Y. (2016), "Keying behavior of gravity installed plate anchor in clay", *Ocean Eng.*, **114**, 10-24. <https://doi.org/10.1016/j.oceaneng.2016.01.018>.
- Muduli, P.K., Das, S.K., Samui, P. and Sahoo, R. (2015),

- “Prediction of uplift capacity of suction caisson in clay using extreme learning machine”, *Ocean Syst. Eng.*, **5**(1), 41-54. <https://doi.org/10.12989/ose.2015.5.1.041>.
- O’Loughlin, C.D., Richardson, M.D., and Randolph, M.F. (2009), “Centrifuge tests on dynamically installed anchors”, *Proceedings of 28th International Conference on Ocean, Offshore and Arctic Engineering*, Honolulu, Hawaii, U.S.A., June.
- O’Loughlin, C.D., Richardson, M.D., Randolph, M.F. and Gaudin, C. (2013), “Penetration of dynamically installed anchors in clay”, *Géotechnique*, **63**(11), 909-919. <https://doi.org/10.1680/geot.11.P.137>.
- Richardson, M.D., O’Loughlin, C.D., Randolph, M.F. and Gaudin, C. (2009), “Setup following installation of dynamic anchors in normally consolidated clay”, *J. Geotech. Geoenviron. Eng.*, **135**(4), 487-496. [https://doi.org/10.1061/\(ASCE\)1090-0241\(2009\)135:4\(487\)](https://doi.org/10.1061/(ASCE)1090-0241(2009)135:4(487)).
- Shelton, J.T., Nie, C. and Shuler, D. (2011), “Installation penetration of gravity installed plate anchors-laboratory study results and field history data”, *Proceeding of the Offshore Technology Conference*, Houston, Texas, U.S.A., May.
- Tian, Y., Cassidy, M.J. and Gaudin, C. (2014), “The influence of padeye offset on plate anchor re-embedding behavior”, *Géotech. Lett.*, **4**(1), 39-44. <https://doi.org/10.1680/geolett.13.00056>.
- Zhao, Y. Liu, H. and Li, P. (2016), “An efficient approach to incorporate anchor line effects into the coupled Eulerian-Lagrangian analysis of comprehensive anchor behaviours”, *Appl. Ocean Res.*, **59**, 201-215. <https://doi.org/10.1016/j.apor.2016.06.005>.
- Zheng, J., Hossain, M.S. and Wang, D. (2015), “New design approach for spudcan penetration in nonuniform clay with an interbedded stiff layer”, *J. Geotech. Geoenviron. Eng.*, **141**(4), 04015003. [https://doi.org/10.1061/\(ASCE\)GT.1943-5606.0001282](https://doi.org/10.1061/(ASCE)GT.1943-5606.0001282).
- Zimmerman, E.H., Smith, M.W. and Shelton, J.T. (2009), “Efficient gravity installed anchor for deep water mooring”, *Proceedings of the Offshore Technology Conference*, Houston, Texas, U.S.A., May.

CC

Notations

- A_p anchor frontal projected area
- D_p anchor frontal projected area equivalent diameter
- $d_{e,t}$ anchor tip embedment (final penetration) depth
- d_t anchor tip penetration depth
- e_n padeye offset distance
- e_p padeye eccentricity
- h_c location of centroid mass
- k shear strength gradient with depth
- L_A anchor shaft length
- s_u undrained shear strength
- $s_{u,ref}$ reference undrained shear strength

- t time after anchor tip impacting seabed
- t_F fin thickness
- v anchor penetrating velocity
- v_i anchor impact velocity
- V_A anchor volume
- W_s anchor submerged weight in water
- z depth below soil surface
- δ_{rem} remoulded strength ratio
- δ_x horizontal displacement
- δ_z loss of embedment depth
- $\dot{\gamma}$ shear strain rate
- $\dot{\gamma}_{ref}$ reference shear strain rate
- η padeye offset ratio
- φ anchor travelling angle
- λ rate parameter for logarithmic expression
- θ_a pullout angle at the padeye
- τ_{max} limiting shear strength at soil-anchor interface
- ξ cumulative plastic shear strain
- ξ_{95} cumulative plastic shear strain required for 95% remoulding